Spectral Characteristics of the Baroclinic Annulus Waves

S. TRIVIKRAMA RAO[1] AND CARL B. KETCHUM[2]

Department of Atmospheric Science, State University of New York at Albany, Albany, N. Y. 12222

(Manuscript received 19 June 1974, in revised form 1 November 1974)

ABSTRACT

This paper reports the results of a statistical study of the temperature field of several examples of regular wave, vacillating flow and irregular flow in a rotating annulus with a gap width of 10 cm using a limited number of thermocouples. The primary results indicate that the regular waves produce several wavenumber harmonics through nonlinear interactions. The wavenumber harmonics decrease in the vacillating flow and are not detectable in the irregular flow. Further, the azimuthal coherence of the flow in the irregular regime decreases very rapidly in azimuth, and yet the vertical coherence is extremely high at all frequencies indicating a strong two-dimensional character of the irregular regime.

1. Introduction

The annulus experiments of Hide (1958) and Fultz *et al.* (1959) have been used to simulate the processes of baroclinic instability which occur in more complicated forms in atmospheric and oceanic circulations. The experiments deal with the thermal convection occurring between two concentric cylinders on a uniformly rotating table. The convection is driven by maintaining the cylinders at different temperatures, and the resulting flow depends primarily on the rotation rate of the turntable, Ω, and the impressed temperature difference ΔT. The flow at low rotation rates is axisymmetric and resembles a Hadley-type circulation. For all but very low impressed temperature differences as the rotation rate increases, the axisymmetric flow becomes unstable and a regular wave pattern appears with a constant drift velocity.

Fowlis and Hide (1965) have shown that the initial occurrence of these waves depends on the Rossby number Θ and the Taylor number $\mathcal{T}$, where

$$\Theta=\frac{g}{\bar{\rho}}\frac{d[\rho(T_a)-\rho(T_b)]}{\Omega^2(b-a)^2},$$

$$\mathcal{T}=\frac{4\Omega^2(b-a)^4}{\bar{\nu}^2}\frac{(b-a)}{d},$$

and d is the depth of the fluid, a and b are the radii of the inner and outer cylinders respectively, $\bar{\rho}$ is the mean density, $\rho(T)$ is the density of the fluid corresponding to the temperature T, T_a and T_b are the temperatures of the inner and outer cylinders, $\bar{\nu}$ is the average value of the kinematic viscosity, and g the acceleration due to gravity.

Fowlis and Hide (1965) and Ketchum (1972) have indicated that the dynamics of the instability that generates the waves closely parallels that of Eady's (1949) theory of baroclinic instability in that the flow is unstable to a given wavenumber m, whenever the Eady number B, given by

$$\mathrm{B}=\frac{g\dfrac{d\rho}{dz}}{4\Omega^2\bar{\rho}}\frac{d^2}{(b-a)^2},$$

is less than a value B_c which is a function of the wavenumber m. At higher rotation rates the regular wave flow becomes unstable and the flow begins to vacillate. At even higher rotation rates the flow is quite irregular.

In this paper the results of power spectral, cospectral and bispectral analysis of the temperature data obtained from four thermocouples located at 0°, 90°, 162° and 280° azimuthal separation at mid-level in the annulus and two additional thermocouples located 5 cm above and below the 280° thermocouple are presented for several runs within the regular wave, vacillation and irregular flow regimes. The range of parameters in Θ, $\mathcal{T}$ space covered in this set of experiments are schematically indicated in Fig. 1. The results are discussed in light of the nonlinear theories of baroclinic instability of Pedlosky (1970, 1971, 1972) and Newell (1972).

[1] Present affiliation: Division of Air Resources Research, New York State Department of Environmental Conservation, Albany.

[2] Present affiliation: College of the Atlantic, Bar Harbor, Maine.

2. Apparatus

a. Convection chamber

The apparatus and the main convection chamber is shown schematically in Fig. 2 and is similar to that described in Ketchum (1972). The specification for the apparatus and the range of parameters for these experiments are listed in Table 1. The main convection chamber is the annular region between two machined aluminum annodized cylinders of inner and outer radii a and b such that the resulting gap width, after careful alignment, is 9.991 ± 0.01 cm. The bottom of the chamber consists of a plane plexiglass adjustable-height false bottom below which fluorescent lights are mounted for dye studies. The depth of the fluid above the false bottom is determined to within ± 0.02 cm with a vernier caliper. A plexiglass lid is placed above the surface, but not in contact with the fluid, to reduce the effects of evaporation and wind stress.

b. Temperature baths

The walls of the convection chamber are maintained at a constant temperature by circulating water at constant but different temperatures through the inner and outer baths. The temperature of the circulating water is maintained constant with time (± 0.05 K) by two Lauda circulators and one cooling unit. A vertical temperature gradient of about 0.05 ΔT exists in each wall due to the tendency of the convecting fluid to have a greater heat transfer near the lower regions of the warm wall and the upper region of the cold wall. This variation is reduced considerably from the original design by forcing most of the circulating water to contact the respective walls at the point of maximum heat transfer. In these experiments the outer wall is always maintained at a higher temperature than the inner wall, and the mean temperature of the two walls is set at room temperature.

Twenty-four thermocouples are placed to within 0.1 cm of the convection chamber side of each wall to monitor the temperature variation within the wall. The temperature difference across the chamber is then determined by the average difference in thermocouple voltage from the thermocouples in each wall spanning the actual region covered by the convecting fluid (18 in each wall for a depth of 20 cm). The average standard deviation of the wall temperatures determined with these thermocouples is 2.3% ΔT and is due primarily to the naturally occurring imposed vertical wall temperature gradient.

c. Turntable

The baths and convection chamber are mounted on a phenolic plate which, in turn, is held above the turntable by three 4-inch machined aluminum I beams. The turntable is formed from $\frac{1}{2}$-inch aluminum stock and is supported by two oppositely directed radial thrust ring bearings mounted on a hollow stainless steel shaft. The hollow shaft, in addition to being the axis of the turntable, also supports electrical power and fluid slip rings.

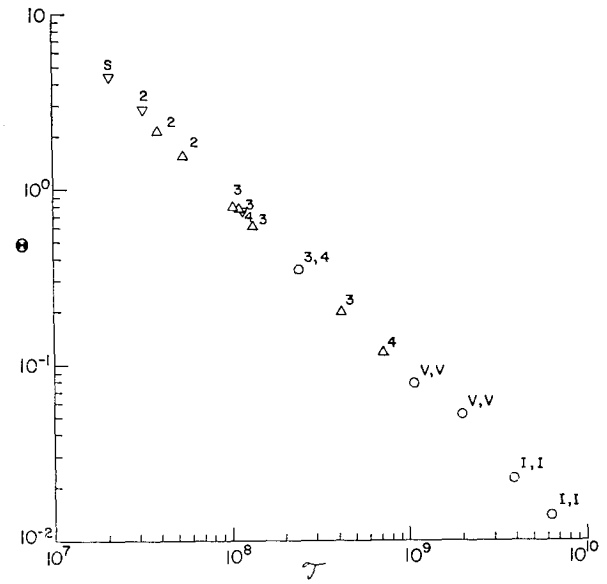

FIG. 1. The physical conditions of the experiments for the A and C series, expressed by the external parameters Θ and $\mathcal{T}$. S denotes the region of axisymmetric flow, numbers 2–4 denote the observed wavenumbers in the regular wave regime, V represents vacillation flow and I the irregular flow. ($\triangle$, run series A; $\triangledown$, run series C; O, run series C and A.)

The turntable is driven by a variable speed Graham transmission unit coupled to the table via a friction O-ring drive. The rotation rate of the turntable is determined by a photoelectric circuit and universal counter triggered by light sources mounted on the table. The rotation rate could be varied from 60 rpm to 0 with a mean short-time stability of 0.08% and a long-term stability of 0.3%.

d. Thermocouple arrays

Two different thermocouple arrays were used in these experiments to determine the azimuthal variations on the wave, vacillating and irregular regime statistics. Array 1, shown in Fig. 3a, consisted of four copper-constantan thermocouples (diameter 0.013 cm) mounted at the center of the convection chamber cross section and placed at 0°, 90°, 162° and 280° in azimuth. At the array position of 280° two additional thermocouples were placed at 5 and 15 cm above the false bottom to determine the vertical stratification. Run series A was completed using this array.

Run series A indicated that coherences in the vacillating and irregular flow were very low even for the smallest azimuthal distance in the array. Thus, a second array (array 2) was designed primarily to explore the

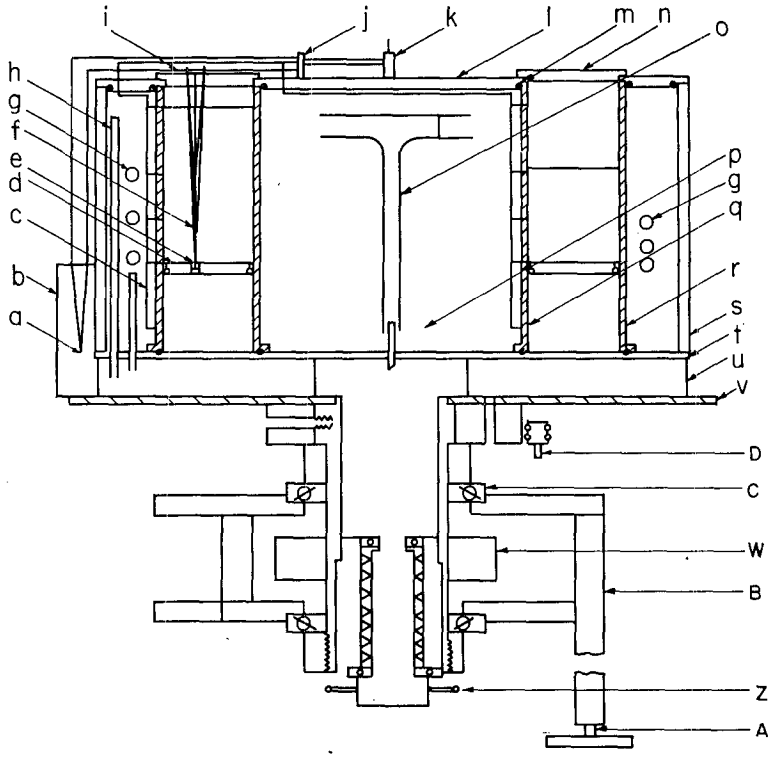

FIG. 2. Section through the apparatus illustrating the general features of its construction. The hatched regions (r and q) are the anodized aluminum walls of the convection chamber. The false bottom of the convection chamber (d) was made of plexiglass as were the cover and the thermocouple mounting blocks (i). The space between (d) and (e), the phenolic base plate, was used to house the fluorescent lamps (not shown). The lids (l) of the temperature baths were sealed to the upper walls of the convection chamber and to the plexiglass outer wall of the whole system (s) by means of O-rings (m). The temperature of each bath was controlled by passing water from constant-temperature circulators (not shown) through perforated copper tubes (g). The return flow from the temperature baths occurred via outflow tubes (p, o) and (h).

Details of the thermocouple array (f) are given in Fig. 3. The common junction of the thermocouple array (a) was placed in the ice bath (b). The array was connected to the external amplifiers, sampling and display units (not shown) via a common miniature plug and slip ring arrangement (j,k). The array was held in position by means of a flush-fitting plexiglass plug (e). The temperatures of the walls of the convection chamber were measured by means of thermocouples (c) mounted in the convection side of the wall.

The phenolic base plate (t) was supported above the horizontal turntable (v) by support blocks (u), thus providing an access to the underside of the temperature baths. The turntable (v) was mounted on a ring bearing (C) supported on a stand (B) with three legs carrying levelling screws (A) sitting in cups on the floor of the laboratory. The water pipes (Z) carried in the inflow and outflow water tubes to the temperature baths. The hollow shaft in addition to being the axis of the turntable also supports electrical power and fluid sliprings (W). The turntable is driven by a variable speed Graham transmission unit (not shown). A steel rod from the transmission unit is attached to the shaft by O-rings (D) which drives the turntable through friction.

variation of the temperature wave coherence over short azimuthal distances. This array consisted of eight thermocouples positioned at the mid point of the chamber cross section in varying azimuthal separations as indicated in Fig. 3b. The minimum separation, for this array, was determined using the smallest discernible eddy size obtained from a time lapse film made in the irregular regime. The other azimuthal positions were set so that integral multiples of this distance could be obtained by looking at the successive combinations of thermocouples. Run series C was completed using array 2.

The convection chamber thermocouples are all referenced to an ice bath located on the turntable, and

TABLE 1. Range of parameters and description.

Parameter	Description	Range	Uncertainty
a	inner radius of the convection chamber (cm)	6.160	±0.003 cm
b	outer radius of the convection chamber (cm)	16.151	±0.003 cm
$b-a$	gap width of the convection chamber (cm)	9.991	±0.010 cm
d	depth of the convecting fluid (cm)	20.00	±0.05 cm
ΔT	temperature difference (T_b-T_a) (K)	$8.4<\Delta T<10.5$	±2%*
$\bar{\nu}$	mean kinematic viscosity (centistokes)	$0.942<\bar{\nu}<0.952$	±0.1%
$\bar{\kappa}$	mean thermometric conductivity ($cm^2\ s^{-1}$)	1.4×10^{-3}	±1%
Ω	rotation rate (s^{-1})	$0.1745<\Omega<5.379$	±0.033%

* Standard error.

the resulting potential difference is carried to the data acquisition systems via a set of low-noise-level slip rings mounted on the top of the turntable. The data could be recorded on two, 2-channel Leeds and Northrup Azor strip chart recorders or on a 20-channel Hewlett Packard digital data acquisition system, with an adjustable sampling rate. The analogue recorders were used primarily for setting up the experiments and all of the analysis was completed using data from the digital data acquisition system which had a sensitivity of 1.3 μV.

e. *Experimental procedure*

In general, the temperatures of the baths were set prior to the start of each series of experiments and held constant during the run series. Each new data point was obtained by changing the rotation rate and allowing the apparatus to reach a mean steady state for at least 12–15 h. Generally the characteristics of the temperature disturbance did not change after the initial 30 min. Analogue recordings were made during the set-up time to check for overnight variations. After set-up, the digital data system was prepared to record at a pre-selected sampling rate for about 4 h in the wave regime and 8–12 h in the vacillating and irregular regimes. The sampling rate was, in general, determined by the frequency resolution required in the spectral calculations as determined by the strip chart recordings. The length of the record was set so that the spectral calculations would have at least 20 degrees of freedom. Within the regular wave regime, the temperature data were recorded with a 1 s sampling interval. The spectral calculations were then based on a 10 s block average of the data, so that the effective sampling interval for the calculations was 10 s. Within the vacillating and irregular regimes the temperature data were recorded at a 10 s sampling interval, and then block-averaged over a 30 or 60 s interval for the calculations as indicated. All of the thermocouple probe temperature data were also nondimensionalized by the impressed temperature difference across the annulus for the respective run.

3. Results

The physical conditions of the experiments discussed in this paper are indicated in Table 2 and schematically shown in Fig. 1. The depth of the fluid in the convection chamber is set at 20 cm and the temperature difference across the convection chamber is kept close to 8.4°C with variations being due to different physical states of the fluid and not to external adjustments. Previous runs at this depth have indicated that the transition from the symmetric to the regular wave region occurs near $\Theta=3.0\pm0.1$ and $\mathcal{T}=(3.1\pm0.2)\times10^7$ for a temperature difference of 9.9°C. The C series runs tabulated in Table 2 indicate that this value of Θ is a little high for the transition to the fully developed wave regime at a temperature difference of 8.4°C; however, our data

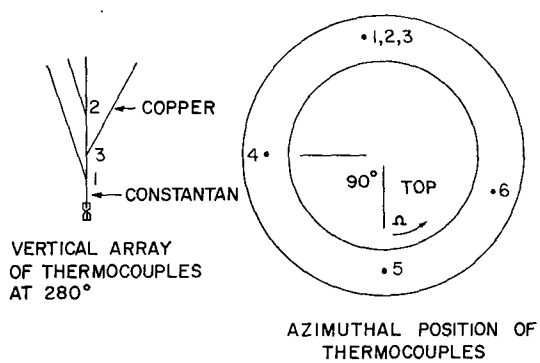

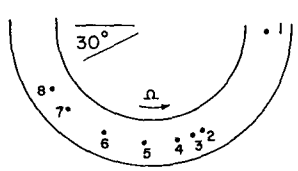

FIG. 3. Diagram illustrating the positions of the thermocouples in the convection chamber. The thermocouples are constructed from 0.0127 cm diameter copper-constantan wire. (a) Thermocouples 3, 4, 5 and 6 are at mid-depth and mid-radius of the annulus. The vertical array 1 and 2 are 5 cm below and above the mid level thermocouple at 280°. The data taken with this set-up form the run series A. (b) The thermocouple array for the run series C. All the thermocouples were placed at the mid-depth and mid-radius of the convection chamber. The azimuthal separation between thermocouples 2 and 3 is 4°9′ (Δ). This separation, arrived at from the time lapse photographs, was found to be the smallest size of a coherent eddy in the irregular regime. This set-up enabled us to determine the variation of coherence for 1 to 20Δ by suitably choosing the thermocouple separations.

TABLE 2. Summary of experimental data for the A and C run series. The state of the flow is indicated by S for the axisymmetric flow and by SA for small-amplitude waves. The wavenumbers observed in the regular wave flow are shown by 2, 3, or 4 with V representing vacillating flow, and I irregular flow. The parameters Θ, $\mathcal{T}$, and B are defined in the Introduction; $E^{-1}=[\mathcal{T}d/(b-a)]^{\frac{1}{2}}$ is the inverse Ekman number. The vertical temperature gradient is determined from thermocouples 1 and 2 which are separated by 10 cm in the vertical. The wave period is obtained from the power spectral results, and the standard deviation is the standard deviation of the dimensional temperature record for the thermocouple 6 for that run.

Run	State	Temperature difference (K)	Rotation rate (s^{-1})	Rossby number Θ	Taylor number $\mathcal{T}$ ($\times 10^9$)	Inverse Ekman number E^{-1} ($\times 10^4$)	Vertical temperature gradient (K cm^{-1})	Eady number B	Wave period (s)	Standard deviation of temperature record
A-2	2	8.39	0.425	2.11	0.0396	0.629	0.335	0.428	239	0.436
A-1	2	8.37	0.498	1.55	0.0546	0.739	0.324	0.301	245	0.494
A-3	3	8.26	0.695	0.788	0.106	1.03	0.311	0.149	159	0.388
A-6	3	8.28	0.701	0.771	0.108	1.04	0.322	0.150	171	0.364
A-7	3	8.25	0.786	0.607	0.136	1.17	0.326	0.122	195	0.347
A-4	3	8.27	1.05	0.346	0.240	1.55	0.323	0.0680	177	0.529
A-5	3	8.30	1.38	0.198	0.420	2.05	0.336	0.0406	230	0.531
A-8	4	8.36	1.80	0.117	0.713	2.67	0.358	0.0255	228	0.510
A-9	V	8.46	2.22	0.0786	1.08	3.29	0.366	0.0171	378	0.516
A-10	V	8.50	3.00	0.0430	1.98	4.45	0.365	0.00935	2440	0.459
A-11	I	8.50	4.17	0.0222	3.89	6.24	0.344	0.00456	—	0.323
A-12	I	8.48	5.25	0.0142	6.06	7.79	0.333	0.00278	—	0.280
C-9	S	8.93	0.307	4.35	0.0208	0.456				
C-8	SA	9.10	0.382	2.86	0.0323	0.569				
C-1	4	8.29	0.890	0.764	0.110	1.05	—	—	111	0.332
C-7	4	8.37	1.040	0.353	0.241	1.55	—	—	130	0.427
C-3	V	8.49	2.23	0.0781	1.10	3.30	—	—	259	0.543
C-4	V	8.54	3.05	0.0418	2.06	4.554	—	—	547	0.487
C-5	I	8.51	4.19	0.0222	3.89	6.24	—	—	—	0.400
C-6	I	8.41	5.38	0.0133	6.40	8.00	—	—	—	0.336

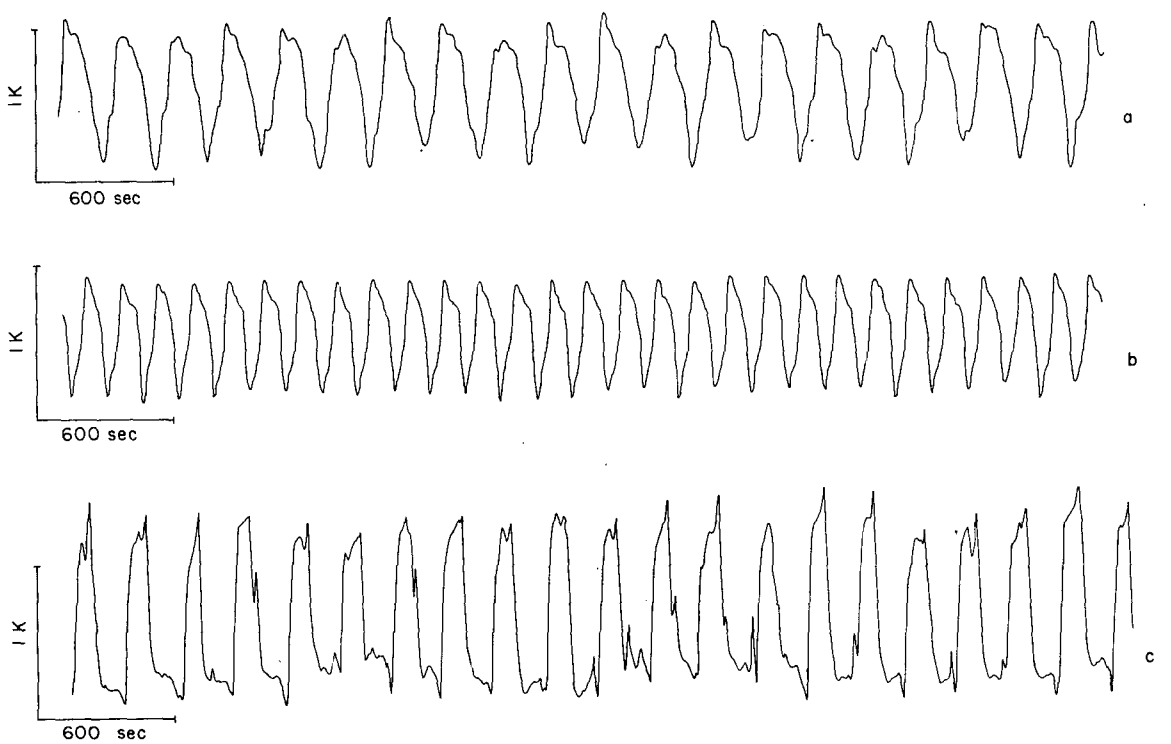

FIG. 4. Typical temperature vs time traces recorded by thermocouple number 6 in array 1 (see Fig. 3a) within the annulus. The length of the line along the time axis (the abscissa) is equivalent to 600 s and that of the line along the temperature axis (the ordinate) to 1 K.

are not sufficiently dense to pinpoint the actual transition. The main thrust of this work will concentrate on the statistical characteristics of the fully developed wave, vacillating and irregular regimes.

A summary of the A series runs which were completed using the thermocouple array 1 is provided in Table 2. Included in Table 2 are the observed wave period, the wavenumber (when it was possible to determine it), the standard deviation of each run which is a good statistical measure of the rms temperature amplitude of the wave disturbance, the vertical dimensional temperature gradient, and the related Eady number B.

Typical temperature traces from thermocouple number 6 in array 1 for a selected series of runs in the A series are reproduced in Fig. 4. Fig. 4a indicates the temperature trace for wavenumber 2 near the transition from the upper symmetric regime to the regular wave regime. Its amplitude is irregular with a stable frequency. This is quite characteristic of the temperature waves that occur near the transition. As the rotation rate is increased, the wave amplitude stabilizes and a regular wave pattern develops which remains stable over many hours (Fig. 4b). At still higher rotation rates the amplitude of the temperature wave fluctuates again, and there is evidence of some higher frequency perturbations but the record still indicates a clear and regular periodic fluctuation (Fig. 4c).

Fig. 4d is an example of wave form (tilted trough) vacillation that occurred at a higher rotation rate than Fig. 4c. The wave period is not as clearly defined in this case and there is strong evidence of significant higher frequencies within the record. Fig. 4e indicates another example of vacillation that occurred at still higher rotation rates. The statistical results indicate that this is an example of wavenumber vacillation. Note that there is a large amount of high frequency within the record, and the wave period is much longer and more irregular than in the other records. At still larger rotation rates, the wave traces lose any resemblance of a regular pattern and this represents irregular flow (Fig. 4f).

The power spectrum estimates for the records from the thermocouple array are obtained using a fast Fourier transform and following the method outlined

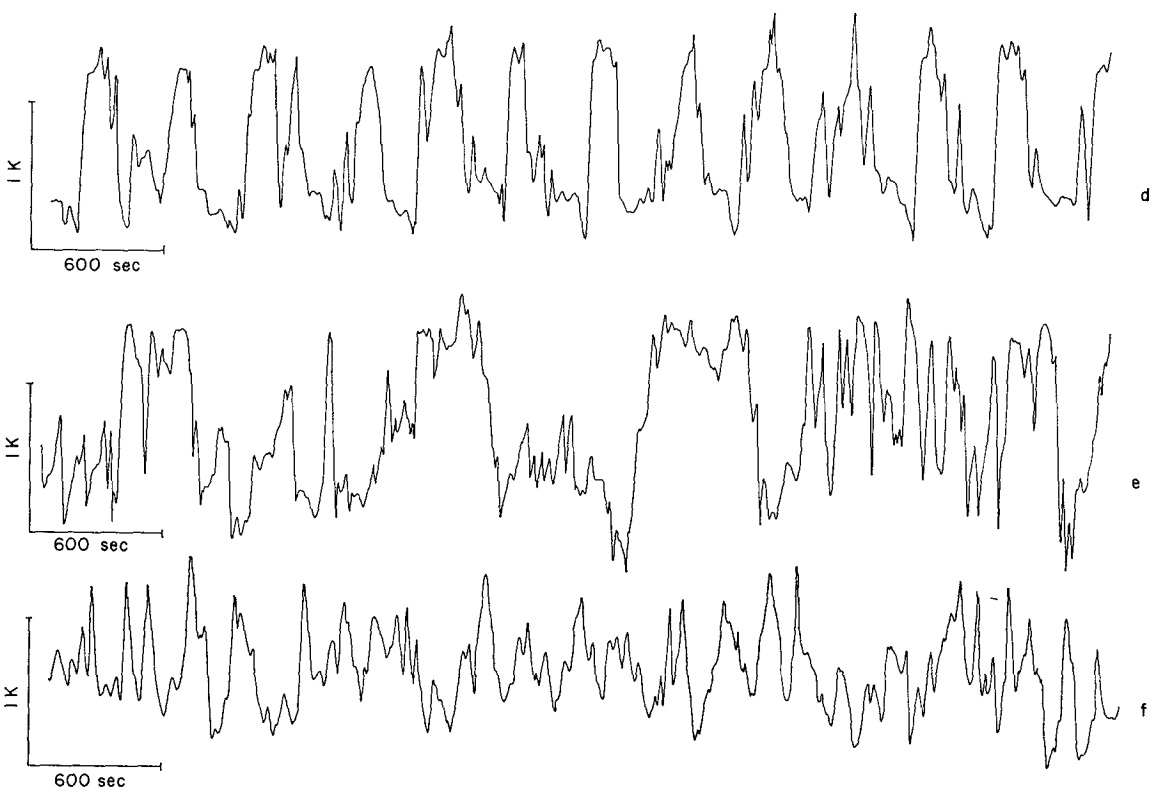

FIG. 4. *Continued.*

Experimental conditions

Fig.	4a	4b	4c	4d	4e	4f
Run	A-2	A-3	A-8	A-9	A-10	A-12
ΔT(K)	8.39	8.26	8.36	8.46	8.50	8.48
$\Omega(s^{-1})$	0.425	0.695	1.80	2.22	3.00	5.25
m	2	3	4	V	V	I

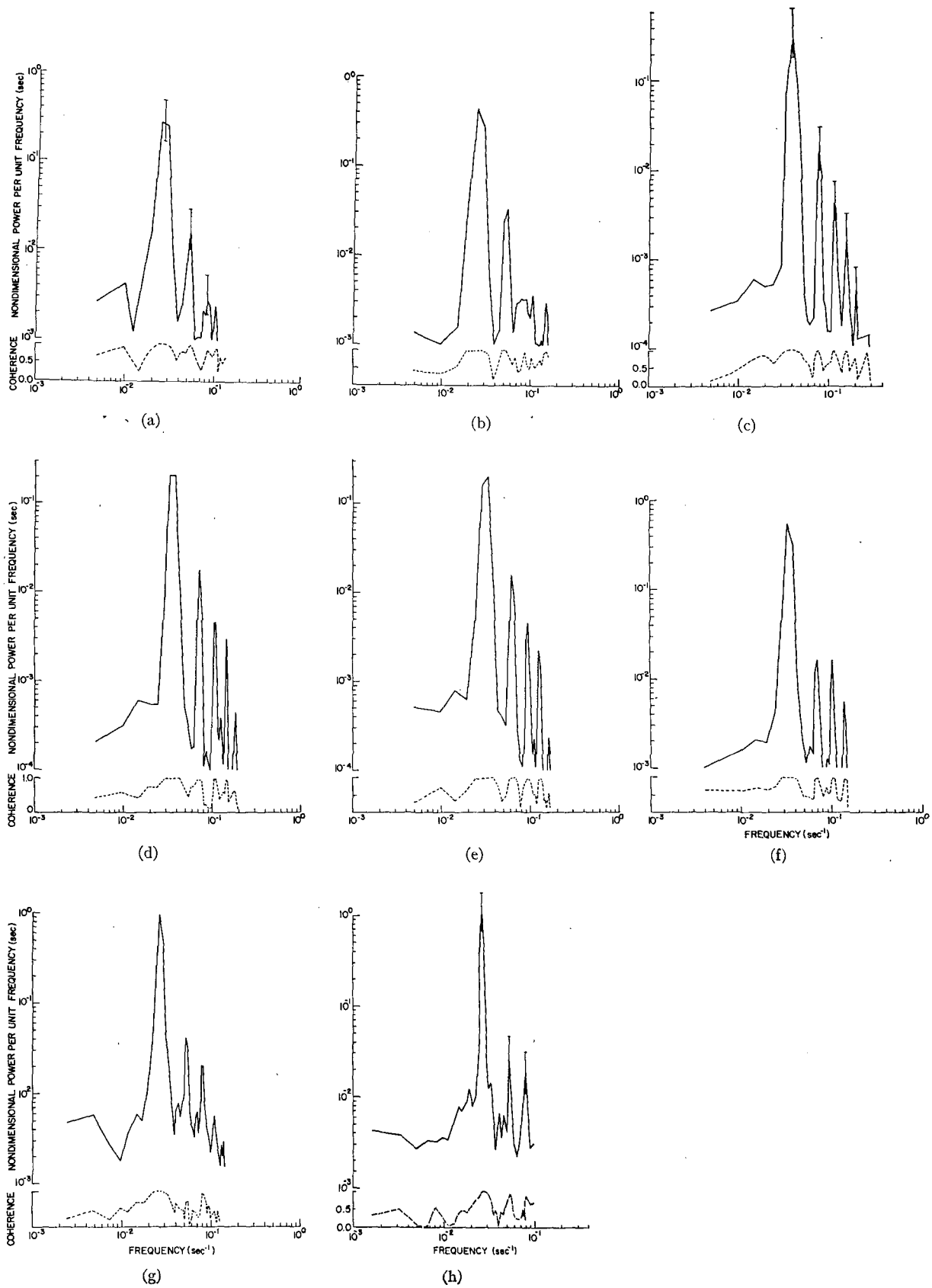

in Hinich and Clay (1968). Essentially, the original record is divided into r equal segments and the Fourier coefficients, $A^i(k)$, $i=1, \ldots, r$, calculated for each of the records at each frequency estimate k. The estimate of the power spectrum $S(k)$ is then given by

$$S(k)=(1/r)\sum_{i=1}^{r}|A^i(k)|^2.$$

This leaves the spectral estimates $S(k)$ with $2r$ degrees of freedom.

In our case each record was subdivided into 10 equal segments; thus, the resulting estimates have 20 degrees of freedom which is sufficient for almost all of the cases discussed herein.

a. Regular wave regime

The temperature power spectra for all of the A series runs in the regular wave regime are presented in Fig. 5. The coherence between two thermocouples separated by 72° is indicated below each spectral plot. Each spectrum has at least one main peak and one highly coherent second harmonic. In most of the records the third and fourth harmonics are also quite significant. In terms of the actual temperature wave amplitude, the spectral results indicate that the first harmonic has an equivalent wave amplitude ranging from 30% (A-6) to 13% (A-8) of the equivalent wave amplitude of the dominant peak, with an average value of 23.2% over the complete series within the wave regime. The higher harmonics are not as clear in the records near the transition from the symmetric to the regular waves (A-2, A-1) and near the transition from the regular waves to the vacillating flow (A-8).

The zonal significance of the spectral peaks is indicated by the coherence between the records obtained from two thermocouples at different azimuthal positions in the annulus. The coherence was calculated from the cross spectrum $S_{xy}(k)$ between the two records x and y which is given (Hinich and Clay, 1968) as

$$S_{xy}(k)=(1/r)\sum_{i=1}^{r}A_x^i(k)A_y^i(k)^*,$$

where the asterisk indicates a complex conjugate. The coherence $\gamma_{xy}(k)$ between the two records at the frequency estimate k is then

$$\gamma_{xy}(k)=|S_{xy}(k)|/[S_x(k)S_y(k)]^{\frac{1}{2}},$$

where the vertical bars indicate the magnitude of the inclosed complex number. A coherence near unity indicates that the relative phase shift between the two records at the frequency estimate k is nearly the same for each of the records, $i=1, \ldots, r$. This, then, is strong evidence for a linear relationship between the two records at this frequency. The variance of the coherence is approximately $(1/2r)[1-\gamma_{xy}{}^2(k)^2]$ and is near zero for γ_{xy} near unity.

The phase of the complex cross spectrum has a variance of approximately $(1/2r)[\gamma_{xy}{}^{-2}(k)-1]$; thus, the phase is highly significant for a coherence near unity. This phase can be used to calculate the azimuthal wavenumber of the spectral peak at the frequency estimate k. Coherence and phase spectra were calculated for angular separations of 72°, 80°, 90° and 118°.

The coherence spectrum for a representative separation is displayed below each power spectral plot in Fig. 5. It is clear that most of the harmonics have a coherence close to unity. This same pattern of coherence is repeated for the separations between the other thermocouples.

The high coherence at the spectral peaks means that the phase spectrum at these peaks can be used to calculate an azimuthal wavenumber for each peak. Typical values of the observed phase and the closest theoretical phase for the wavenumber are shown in Table 3 for runs A-2, A-3 and A-8. For a population coherence of 0.9 and 20 degrees of freedom the 95%

TABLE 3. The results of the spectral analysis of series A in the regular wave regime.

Run	Harmonic	Frequency	Coherence	Observed phase for separation of 118°	Harmonic wavenumber	Theoretical phase
A-2	0	0.0245	0.998	−2.09	2	−2.16
		0.0295	0.999	−2.09		
	1	0.054	0.983	2.14	4	1.95
	2	0.081	0.696	−0.13		
		0.088*	0.721	−0.43	6	−0.21
		0.093	0.741	−0.28		
	3	0.108	0.807	−2.40	8	−2.37
A-3	0	0.039	0.999	0.02	3	−0.11
	1	0.078	0.991	−0.56	6	−0.21
	2	0.117	0.939	−0.09	9	−0.31
	3	0.157	0.972	−0.34	12	−0.42
	4	0.196	0.905	1.84	?	−0.52
A-8	0	0.028	0.999	−0.09**	4	0.0
	1	0.056	0.944	0.00	8	0.0
	2	0.083	0.890	−0.01	12	0.0

* As indicated in Fig. 5a the peak at 0.081 is smaller than a neighboring peak at 0.088 and 0.093 and both points have been included for completeness.

** The numbers given represent the observed phase for a separation of 90°.

FIG. 5. Power spectral density estimates for the run series A: (a) run A-2, (b) run A-1, (c) run A-3, (d) run A-6, (e) run A-7, (f) run A-4, (g) run A-5, (h) run A-8. The coherence plotted underneath corresponds to a separation of 72° in the azimuthal direction. The effective sampling interval for these calculations is 10 s. The 90% confidence interval for the 20 degrees of freedom is set by a chi-squared distribution and is indicated in the figures at the peak. If $S(f_K)$ is the true spectral estimate and S_K the estimated value, then there is a 90% confidence (for 20 degrees of freedom) that $0.65\,S_K<S(f_K)<1.8S_K$. A dimensional spectral density can be obtained from our results by multiplying the given density by the square of the impressed temperature difference for that run.

TABLE 4. The results of the bispectrum analysis of series A in the regular wave regime.

Run	Harmonic interaction	Interacting frequencies $\omega_{(j)}$	$\omega_{(k)}$	Resulting frequency $\omega_{(j+k)}$	Skewness
A-2	0+0 → 1	0.0245	0.0245	0.049	0.89
		0.0295	0.0245	0.054	0.98
		0.0295	0.0295	0.059	0.91
	0+1 → 2	0.0245	0.054	0.079	0.60
		0.0295	0.054	0.083	0.47
	1+1 → 3	0.054	0.054	0.108	0.91
A-3	0+0 → 1	0.039	0.039	0.078	1.00
		0.039	0.044	0.083	0.99
	0+1 → 2	0.039	0.079	0.118	0.96
		0.039	0.083	0.122	0.95
		0.044	0.079	0.122	0.94
	0+2 → 3	0.039	0.118	0.157	0.94
		0.039	0.123	0.162	0.92
	1+1 → 3	0.079	0.079	0.158	0.98
		0.079	0.083	0.162	0.98
A-8	0+0 → 1	0.026	0.028	0.054	0.90
		0.028	0.028	0.056	0.95
	0+1 → 2	0.028	0.056	0.084	0.88

confidence level on the phase is 0.225 rad. Most of the results indicate that, at this level, the results for all of the runs are consistent with the observation that the higher frequency harmonics also correspond to wavenumber harmonics in the azimuthal direction. Note that the second harmonic in A-2 is not a really significant peak and, as such, has a low coherence. The third harmonic is much stronger and does indicate reasonable coherence. In A-3 the harmonic peaks agree well up to the fourth harmonic, although the fourth harmonic does not correspond in phase to wavenumber 15. However, for the high wavenumbers the angular spacing becomes critical and could, in this case, introduce a major part of the discrepancy. When the coherence is greater than 0.9, the 95% confidence interval decreases, and the results really should show better agreement than is indicated in this table. For example, the first harmonic in A-3 has an observed phase of −0.56 rad and wavenumber 6 should have a phase difference of −0.21 rad indicating a discrepancy of 0.35 rad. Wavenumber 6 is indicated in this case since

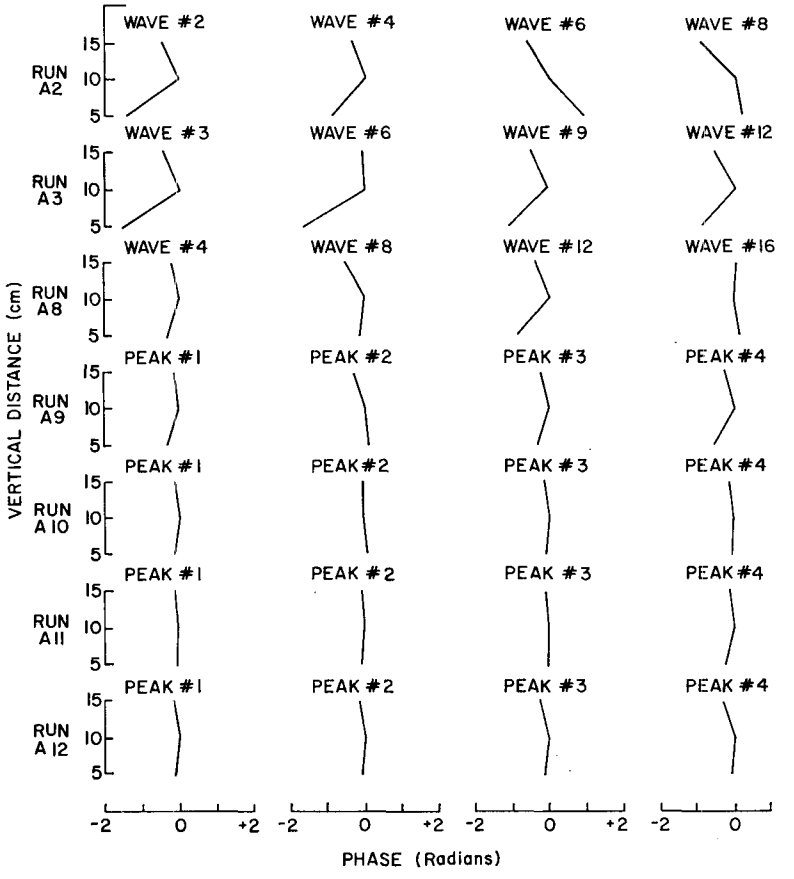

FIG. 6. Vertical variation of the phase at 280° in the annulus. The curve on the extreme left corresponds to the observed wavenumber (first peak in the spectral density estimate) in a run and to its right are the harmonics (the other distinct peaks in the spectral density estimate) of the observed wavenumber. From run A-9 onward the curves correspond to the peaks in the power spectra, as those peaks no longer represent a definite wavenumber.

all the surrounding possible wavenumbers would introduce a much larger discrepancy.

The extent to which the higher harmonics in the spectra for the regular wave regime are due to nonlinear interactions between the lower harmonics can be estimated by the skewness of the bispectrum. The bispectrum is computed as

$$B(j,k)=(1/r)\sum_{i=1}^{r} A^i(j)A^i(k)A^i(j+k)^*$$

and the skewness is given by

$$\hat{\rho}(j,k)=|B(j,k)|/[S(j)S(k)S(j+k)]^{\frac{1}{2}}.$$

The skewness of the bispectrum is essentially the coherence between the observed spectral component at the frequency $\omega(j+k)$ and the resulting spectral components computed from postulated nonlinear interaction between any two other peaks at frequencies of $\omega(j)$ and $\omega(k)$ such that $\omega(j)+\omega(k)=\omega(j+k)$. The computed interaction spectrum for $\omega(j+k)$ is the product of the two observed complex spectral estimates of frequencies $\omega(j)$ and $\omega(k)$. Thus, a skewness of unity indicates the strong possibility of nonlinear interaction producing the spectral estimate at a frequency of $\omega(j+k)$.

The results of the bispectral computations for the significant peaks in each spectrum for runs A-2, A-3 and A-8 are presented in Table 4. The high value of the skewness at the harmonic peaks in the spectrum are consistent with the assumption that the higher harmonics in the spectrum are the results of nonlinear interactions between temperature disturbances at lower frequencies. The interactions involving frequencies $[\omega(k)-\omega(j)]$ were also computed, and the skewness for all the frequencies lower than the significant peaks was less than 0.8, indicating little transfer of energy toward the low-frequency side of the spectrum.

Thermocouples 1, 2 and 3 can be used to obtain the vertical phase of the wave disturbances at 5, 10 and 15 cm above the bottom of the annulus. This information, presented in Fig. 6, indicates that the phase of the wave, due to the dominant peak, leads in the upper region of the fluid for low rotation rates, and has almost no vertical phase shift at the higher rotation rates.

At the suggestion of one referee, the spectral results for run A-3 were used to develop a picture of an average wave for the thermocouples at the 5, 10 and 15 cm depths; the results are given in Fig. 7.

The average wave is found by superimposing all the wave cycles in a thermocouple record and then averaging the specific value for each phase of the wave to find the shape of the averaged wave. These shapes indicate the amplitude and phase relationships of the locked-in harmonics that are not available in the spectral presentations. The three waves, indicated in Fig. 7, also show the average phase relationship of the waves in the vertical at one azimuthal point. It is clear that the phase of the temperature wave in the upper region of the fluid leads that of the temperature wave at the lower thermocouple, indicating that, in the azimuthal direction, the trough slopes upward toward the direction of rotation, i.e., eastward.

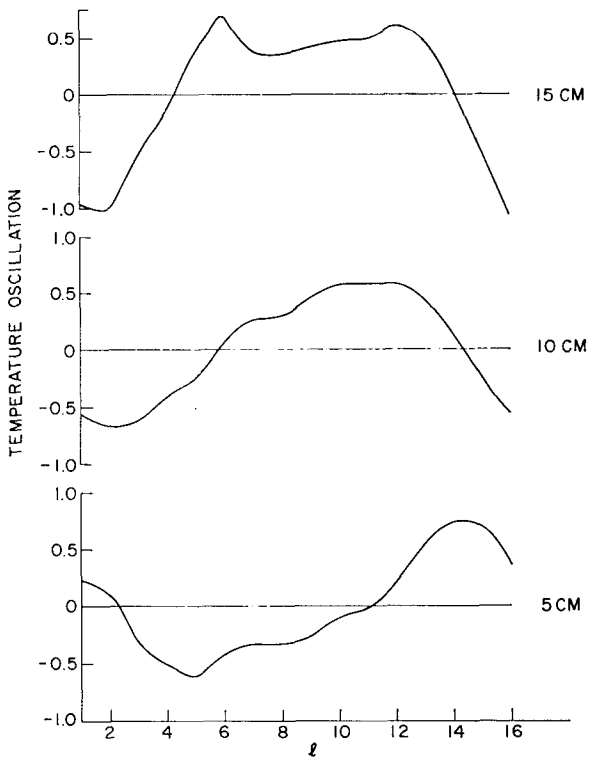

FIG. 7. The shape of the temperature wave through a superposition of many wave cycles for run A-3 at 280°. The wave has a period of 160 s. The averaging over a wave period is done as follows. If $T(J)$, $J=1$, n, is a long record of total length n having a wave period τ, and the data are sampled at intervals of Δt, then

$$K=\frac{\tau}{\Delta t}\,(\text{integer})=\frac{160}{10}=16\ (\text{in the present case}).$$

The averaging is done by

$$\bar{T}(l)=\sum_{m=1}^{n/K} T[l+(m-1)K],\quad \text{for } l=1,\ldots,K.$$

b. *Vacillating and irregular regimes*

The temperature spectra and coherence for an angular separation of 72° for the A series runs in the vacillation and irregular regimes are shown in Fig. 8. All of the spectral results for the vacillation regime were made from data sampled at a 10 s interval and block-averaged to give an effective sampling interval of 30 s. The power spectral results for the irregular regime shown in Fig. 8 were also computed using the effective sampling interval of 30 s. The other results indicated for the irregular regime were obtained from data with an effective sampling interval of 60 s.

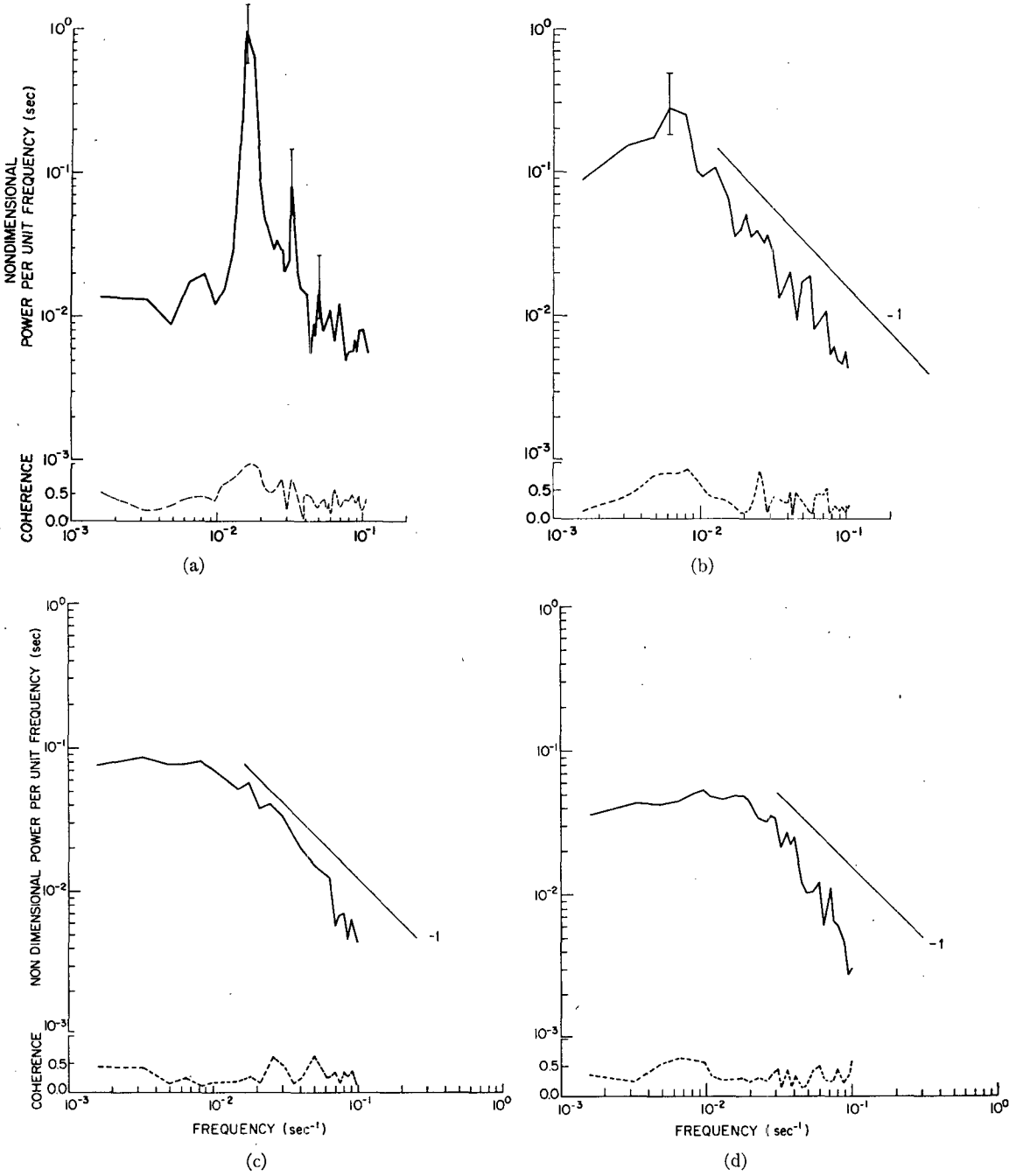

FIG. 8. Power spectral density estimates: (a) run A-9, (b) run A-10, (c) run A-11, (d) run A-12. The coherence plotted for A-9 and A-10 is for an azimuth angular separation of 72° and for A-11 and A-12, 90°. The effective sampling interval for these calculations is 30 s. The 90% confidence interval for the 20 degrees of freedom is set by a chi-squared distribution and is indicated in the figures at the peak. If $S(f_K)$ is the true spectral estimate and S_K the estimated value, then there is a 90% confidence (for 20 degrees of freedom) that $0.65\ S_K < S(f_K) < 1.8\ S_K$. A dimensional spectral density can be obtained from our results by multiplying the given density by the square of the impressed temperature difference for that run.

The sharp spectral peak of the dominant frequency, so apparent in the regular wave regime, is only clearly seen in run A-9. As the rotation rate is increased, the main peak broadens (A-10), and finally disappears in the irregular regime (A-11 and A-12). The high-frequency end of the spectra for runs A-10, A-11 and A-12 have slopes nearly proportional to f^{-1}. A more detailed discussion of the individual spectra follows.

There are two significant peaks in the spectrum for run A-9 with coherence of 0.99 and 0.87 for the lower

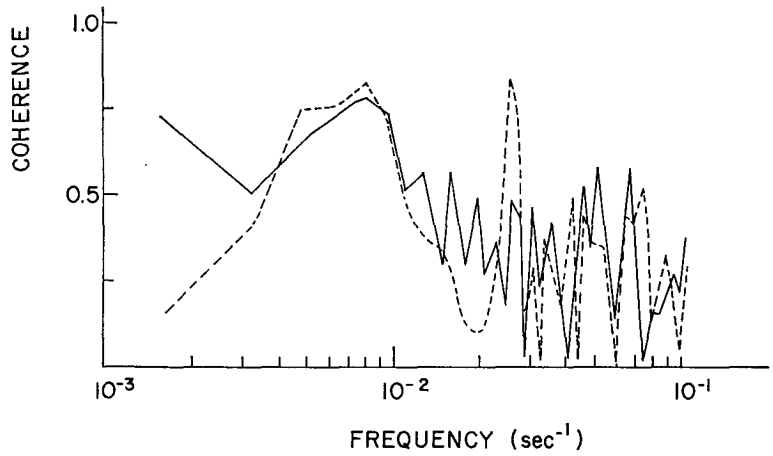

FIG. 9. Variation of coherence with frequency for run A-10. Dashed lines correspond to an azimuthal separation of 80° and solid lines to a separation of 118°.

and higher frequency peaks respectively. The phase information indicates that the dominant peak is close to wavenumber 4 with a discrepancy of 0.25 rad, and the second peak is close to wavenumber 8 with a discrepancy of 0.38 rad. In addition, the bispectral results show a skewness of 0.91 for the self-interaction of the dominant peak producing the next harmonic at the second peak. Thus, this example has retained some of the characteristics of the wave regime spectra, but the main peak occurs at a much lower frequency. In addition, the temperature traces for run A-9 as indicated in Fig. 4d indicates a much more irregular pattern. The spectra for A-10 indicates no clear-cut harmonics. However, the coherence for a separation of 80° is greater than 0.82 at two points in the spectrum, and the phase information at these points indicates the presence of wavenumbers 5 and 6 at the frequencies 0.0065 and 0.026 s^{-1}, respectively, indicating the possibility of a wavenumber vacillation. Fig. 9 presents the variation of coherence in this run with frequency for the angular separation of 80° and 118°. It is clear that the second peak in the coherence spectrum decreases significantly at 118°. The bispectral results for A-10 do not indicate any significant skewness over 0.7 for all frequencies in the spectrum.

The spectra with a 30 s sampling interval for runs A-11 and A-12 in the irregular regime indicate a slope proportional to the inverse frequency at the high-frequency end. The spectra calculated with a 60 s sampling interval were flatter and had a much less pronounced slope. The coherence for each of these runs is much less than 0.7 in almost all cases, and, as such, it is impossible to indicate the zonal structure of this regime. The coherence and phase spectrum for a vertical separation of 10 cm is shown in Fig. 10 for run A-12. This result indicates that over this vertical distance the motion is highly coherent and has almost no phase shift.

The lack of azimuthal coherence in the vacillating and irregular flows prompted a second series of experiments using an array designed to have a minimum separation of one-half of the smallest observed wavelength in the irregular flow. Time lapse photographs of the irregular flow indicated that this separation distance was 4°9′ in azimuth, and array 2 was then constructed so that separation distances of from 1Δ to 20Δ could be obtained with Δ set at 4°9′. Run series C (see Table 2) was then taken to duplicate as nearly as possible some of the points from run series A with the new array. However, the wavenumber of the C series run may not duplicate the same wavenumber in the A series run since the wavenumbers are not always reproducible, and small changes in the impressed temperature difference and rotation rate can also affect the wavenumber present. The spectral results for these series are similar to those presented in the previous section for run series A. The closer spacing of the thermocouples enable us to make a much clearer statement as to the variation of coherence over angular

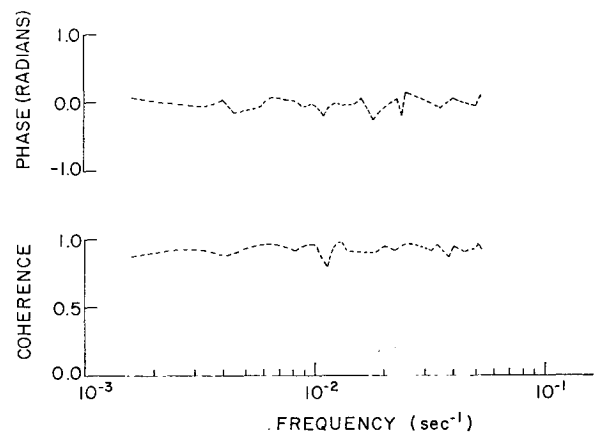

FIG. 10. Coherence and phase variation for a vertical separation of 10 cm for run A-12. These calculations are based on data with an effective sampling interval of 60 s.

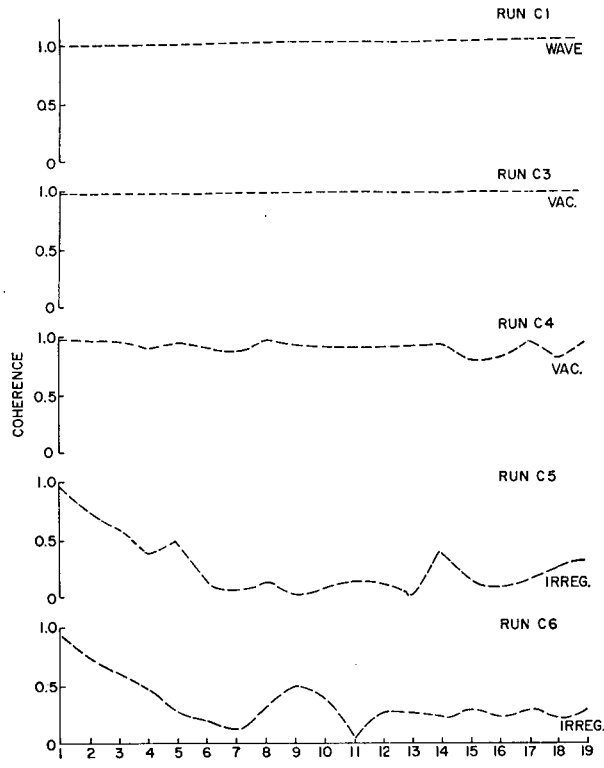

FIG. 11. Coherence variation corresponding to the first peak in the power spectra with grid spacing $\Delta = 4°9'$ for all regimes. The computations for the irregular flow are based on data with an effective sampling interval of 60 s.

separation of from 4°9′ to 83° (1Δ to 20Δ). Since we are interested in the qualitative nature of the irregular flow through array 2, the increased probe effects should not unduly bias the conclusions. Fig. 11 shows a plot of the coherences of the spectral peak with the most power as a function of the angular separation. C-1 represents a point in the regular wave and the coherence is almost unity for all separations. C-3 represents the first point in the vacillation regime which still retains a dominant and sharp peak as in Fig. 8a. The coherence in this case is still close to unity for all separations. As the rotation rate is increased, however, the coherence for C-4 in the vacillation regime and C-5 and C-6 in the irregular flow regimes decreases in general with increasing separation.

The variation of coherence for separations of 1, 2 and 3Δ over all frequency for the irregular regime point C-6 is indicated in Fig. 12. This indicates further that the coherence drops off rapidly for all frequencies in the irregular flow. In fact, the average coherence over all frequencies for this run is 0.8, 0.55 and 0.4 for separations of 1, 2 and 3Δ, respectively.

4. Discussion and conclusion

The results of the studies in the regular wave regime indicate a clear nonlinear maintenance of the fundamental wave and its harmonics in the equilibrated state. The existing theories of nonlinear baroclinic instability (Pedlosky, 1970, 1971, 1972; Newell, 1972) in a two-layer baroclinic fluid do not show the generation of higher harmonics. Several factors in the annulus experiments not considered in the above studies, namely, the circular geometry, the shape of the free surface, and the radial variation of zonal velocity of the basic state, may be responsible for the generation of higher harmonics. The shape of the upper surface can be changed with a rigid lid, in which case the preliminary results still indicate the presence of higher harmonics, implying that the other two factors are more likely responsible for this development.

Pedlosky (1970) indicated that when the flow is effectively inviscid, the baroclinic waves do not reach a steady state but continuously pulsate with time indicating a type of amplitude vacillation. An estimation of the critical parameter by Ketchum (1972) indicated that the effectively inviscid region for the annulus would occur near the transition from the symmetric to the regular wave regime. We suspect that the amplitude vacillation of the wave, visible in Fig. 4a, may be due to this process.

The wavenumber harmonics, so apparent in the regular waves, decrease in significance in the vacillating flow and vanish altogether in the irregular flow. The azimuthal coherence for the vacillating flow over a distance of 20Δ in run series C, shown in Fig. 10, does indicate that the vacillation cases resemble the regular wave regime more than they do the irregular regime. However, the coherences drop off for separation distances beyond 20Δ while in the regular wave cases the motions are highly coherent all around the annulus. The azimuthal coherence of the temperature fluctuations in the irregular regime decreases very rapidly with increasing separation. However, the vertical coherence in these cases is very high with almost no phase shift over the half of the fluid spanned by the

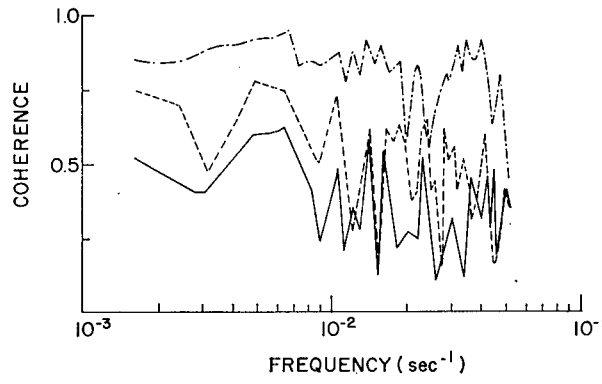

FIG. 12. The variation of coherence with frequency for run C-6. These calculations are based on data with an effective sampling interval of 60s. (Dot-dashed line, separation 1Δ; dashed line, 2Δ; solid line, 3Δ.)

vertical array. Thus, the irregular flow has the formal characteristics of a two-dimensional turbulent fluid. The spectra near the high-frequency end have a slope proportional to the -1 power of the frequency (see Figs. 8b–8d), results that are similar to those of Kao (1970) in the atmospheric case. Most of the theories of two-dimensional turbulence (Batchelor, 1969; Leith, 1971) and of quasi-geostrophic turbulence (Charney, 1971) predict results in terms of the wavenumber spectrum. It is difficult for us to transform our results to a wavenumber spectrum. If the temperature field were frozen into the flow and simply advected by the thermocouple probe, the wavenumber spectrum would also have a -1 dependence on the wavenumber, but this does not appear to be a valid assumption from our observations of the film of this regime.

It would be interesting to obtain a direct spectra dependent on the wavenumber for the irregular flow in the annulus, but this would require a great many more probes than we have the facilities for. Our results do indicate that the irregular flow in the annulus could provide a direct analog verification of some of the two-dimensional turbulence theories. It is also possible that higher order spectral calculations may indicate the presence of cubic and higher nonlinear interactions occurring in this regime when the quadratic interactions are not detectable.

Acknowledgments. The authors wish to thank Mrs. Joyce Elia for typing the manuscript and Mrs. Marilyn Peacock for drafting the diagrams. Thanks are extended to the referees for their valuable comments which improved the quality of the presentation of the results. This study was supported by the National Science Foundation under Grant GA-12734.

REFERENCES

Batchelor, G. K., 1969: Computation of the energy spectrum in the homogeneous two-dimensional turbulence. *Phys. Fluids*, Supp. II, 233–239.

Charney, J. G., 1971: Geostrophic turbulence. *J. Atmos. Sci.*, **28**, 1087–1095.

Eady, E. T., 1949: Long waves and cyclone waves. *Tellus*, **1**, 33–52.

Fowlis, W. W., and R. Hide, 1965: Thermal convection in a rotating annulus of liquid: Effect of viscosity on the transition between axisymmetric and non-axisymmetric flow regimes. *J. Atmos. Sci.*, **22**, 541–558.

Fultz, D., R. R. Long, G. V. Owens, W. Bohan, R. Kaylor and J. Weil, 1959: Studies in thermal convection in a rotating cylinder with sone implications for large-scale atmospheric motions. *Meteor. Monogr.*, **4**, No. 21, 1–104.

Hide, R., 1958: An experimental study of thermal convection in a rotating fluid. *Phil. Trans. Roy. Soc. London*, **A250**, 441–478.

Hinich, M. J., and C. S. Clay, 1968: The application of the discrete Fourier transform in the estimation of power spectra, coherence, and bispectra of geophysical data. *Rev. Geophy.*, **6**, 347–363.

Kao, S. K., 1970: The wavenumber frequency spectra of temperature in the free atmosphere. *J. Atmos. Sci.*, **27**, 1000–1007.

Ketchum, C. B., 1972; An experimental study of baroclinic annulus waves at large Taylor number. *J. Atmos. Sci.*, **29**, 665–679.

Leith, C. E., 1971: Atmospheric predictability and two-dimensional turbulence. *J. Atmos. Sci.*, **28**, 145–161.

Newell, A. C., 1972: The post bifurcation stage of baroclinic instability. *J. Atmos. Sci.*, **29**, 64–76.

Pedlosky, J., 1970: Finite-amplitude baroclinic waves. *J. Atmos. Sci.*, **27**, 15–30.

——, 1971: Finite-amplitude baroclinic waves with small dissipation. *J. Atmos. Sci.*, **28**, 587–597.

——, 1972: Limit cycles and unstable baroclinic waves. *J. Atmos. Sci.*, **29**, 53–63.